2009

Simulation of a Tubular Solid Oxide Fuel Cell Stack Operating on Biomass Syn-gas using Aspen Plus

Wayne Doherty
Technological University Dublin, wayne.doherty@tudublin.ie

Anthony Reynolds
Technological University Dublin, anthony.reynolds@tudublin.ie

David Kennedy
Technological University Dublin, david.kennedy@tudublin.ie

Recommended Citation

W. Doherty, A. Reynolds, D. Kennedy. Simulation of a Tubular Solid Oxide Fuel Cell Stack Operating on Biomass Syn-gas Using Aspen Plus. ECS Transactions 2009;25:1321-1330 (presented at: 216th ECS Meeting: Solid Oxide Fuel Cells, Eleventh International Symposium (SOFC-XI), Vienna, Austria, 2009). doi:10.1149/1.3205661

ECS Transactions, 25 (2) 1321-1330 (2009)
10.1149/1.3205661 ©The Electrochemical Society

Simulation of a Tubular Solid Oxide Fuel Cell Stack Operating on Biomass Syn-gas using Aspen Plus

W. Doherty, A. Reynolds, and D. Kennedy

Department of Mechanical Engineering
Dublin Institute of Technology, Bolton Street, Dublin 1, Ireland

A tubular solid oxide fuel cell (SOFC) stack is modelled and its operation on biomass syn-gas is investigated. The objective of this work is to develop a computer simulation model of a biomass gasification-SOFC (BG-SOFC) system capable of predicting performance under various operating conditions and using diverse fuels. The stack is modelled using Aspen Plus and considers ohmic, activation and concentration losses. It is validated against published data for operation on natural gas. Operating parameters such as fuel and air utilisation factor (U_f and U_a), current density (j) and steam to carbon ratio ($STCR$) are varied and have significant influence. The model is run on wood and miscanthus syn-gas. The results indicate that there must be a trade-off between voltage, efficiency and power with respect to j and the stack should be operated at low $STCR$ and high U_f. High efficiencies are predicted making these systems very promising.

Introduction

As the contribution of renewable energy increases, biomass is likely to play an important role as it is among the most promising sources of renewable energy in the context of both environmental and energy security issues. Traditionally, energy is recovered from biomass through combustion at low electrical efficiency (20-25%). Biomass gasification systems offer much higher efficiencies thus making the fuel suitable for power generation. Biomass gasification is well suited for integration with high temperature fuel cells. Reported electrical efficiencies for biomass gasification-solid oxide fuel cell (BG-SOFC) systems range from 23-50% (1). These systems offer highly efficient renewable energy and are modular in nature making them ideal for decentralised combined heat and power (CHP) applications and as a result have recently gained much attention (2-7).

SOFCs convert the chemical energy contained in a fuel gas directly to electrical energy via electrochemical reactions, making them a highly efficient energy conversion device. The tubular SOFC configuration is considered to be the most advanced and therefore was selected for this study. This technology was developed by Siemens Power Generation Inc (SPGI). These SOFCs can utilise a wide spectrum of fuels (natural gas, coal and biomass syn-gas) due to their high operating temperature. Various models have been developed to simulate tubular SOFC performance, many of them for operation on humidified H_2 or natural gas (8-11). A review of SOFC models can be found in the literature (12). In this work the operation and performance of a tubular SOFC stack on wood and miscanthus syn-gas was investigated. Sensitivity analyses were carried out in order to give insight into the influence of the main variables on the system.

Technology Description

Biomass Gasification Systems

The Güssing biomass CHP plant utilises 8 MW of wood chip fuel to produce 2 MW_e of electricity (grid connected) by means of a gas engine and 4.5 MW_{th} of heat (district heating system). The wood syn-gas is produced using an atmospheric pressure dual fluidised bed (DFB) steam gasifier. A detailed description of the process can be found in the literature (5, 13). Efforts are ongoing to get a SOFC stack installed for testing at the Güssing plant (14). The following syn-gas composition was inputted to the SOFC stack model: 45.8% H_2, 21.6% CO, 10.0% CH_4, 21.2% CO_2, 1.4% N_2 (vol. %, dry basis) and 25.7% H_2O (vol. %, wet basis) (5).

Numerous experiments have been carried out at the Delft University of Technology using a pilot scale 100 kW_{th} atmospheric pressure circulating fluidised bed (CFB) gasifier. Experiments have been conducted using a wide range of fuels, including various woods, miscanthus and straw. Reported syn-gas compositions from these experiments for miscanthus gasification have been used in this work: 13.65% H_2, 21.6% CO, 7.5% CH_4, 2.0% C_2H_y, 35.25% CO_2, 13.0% N_2 (vol. %, dry basis) (15) and 40% H_2O (vol. %, wet basis) (16). This miscanthus syn-gas was produced using a steam-oxygen mixture as fluidising agent and plain sand as bed material.

SOFC Stack

The 100 kW AC CHP tubular SOFC stack developed by SPGI was selected and modelled. The operation of the stack is as follows: the oxidant stream is fed via injector tubes, placed centrally in each SOFC, to the closed end of the cells. The oxidant then flows back through the annular space formed by the cathode surface and the injector tube to the open end. The oxidant is electrochemically reacted with the fuel supplied to the anode as it flows over the cathode surface. Cleaned fuel gas is supplied to the ejector where it is mixed with depleted fuel from the recirculation plenum. This anode recycle loop provides the steam and heat required for the steam reforming process. The mixed fuel then passes through the pre-reformers which convert the higher hydrocarbons and a small portion of the CH_4 adiabatically to H_2 and CO. The partially reformed fuel enters the internal reformers and using the heat generated by the exothermic electrochemical reactions occurring in the SOFC stack it is reformed further. The fuel then flows along the anode surface from the closed end to the open end, parallel to the direction of the oxidant flow and is electrochemically oxidised, generating electricity and increasing the temperature of both streams. A portion of the depleted fuel is recycled, the quantity of which depends on the required steam to carbon ratio (*STCR*) and the remainder is reacted with the depleted oxidant in the combustion plenum. The generated heat serves to preheat the incoming oxidant stream in the injector tubes. The high temperature exhaust gas may then be utilised in a district heating system.

SOFC Stack Model

Model Flowsheet Description

With reference to Figure 1, the stream ‘SYN-GAS’ is fed to the ‘COMP1’ block, the fuel compressor and its discharge pressure was set by assuming a pressure ratio:

P_{fuel}/P_{SOFC} = 3 (9). Syn-gas composition and thermodynamic condition were inputted; its mole flow rate depends on the specified stack power (or for variable power it is set depending on the specified current density (j)). The syn-gas is preheated in the block 'FUELHEAT' and its exit stream enters the 'EJECTOR', where it is mixed with the recycled depleted fuel. The pressure of stream 4 is decreased to slightly above atmospheric pressure (P_{SOFC}) and is directed to 'COOLER1'. The two blocks 'COOLER1' and 'PREREFOR' represent the stack pre-reformers. 'COOLER1' sets the pre-reforming temperature, which is calculated by means of a design spec, which varies the temperature of 'COOLER1' until the net heat duty of 'PREREFOR' equals zero, i.e. adiabatic. The gas is cooled simulating the endothermicity of the steam reforming process. The following chemical reactions, assumed to reach equilibrium, were specified in the 'PREREFOR' block:

Steam reforming:	$C_nH_m + nH_2O \leftrightarrow (m/2 + n)H_2 + nCO$	[1]
Water-gas shift:	$CO + H_2O \leftrightarrow CO_2 + H_2$	[2]

The pre-reformed fuel (stream 6) enters 'ANODE', where the remaining CH_4 is reformed, CO is shifted and H_2 is oxidised. In a SOFC the following reactions occur:

Cathode half reaction:	$0.5O_2 + 2e^- \rightarrow O^{2-}$	[3]
Anode half reaction:	$H_2 + O^{2-} \rightarrow H_2O + 2e^-$	[4]
Overall reaction:	$H_2 + 0.5O_2 \rightarrow H_2O$	[5]

The oxygen ion O^{2-} is the charge carrier in a SOFC. It is transported through the electrolyte to the anode side where it reacts with H_2 to produce electrons e^-. This cannot be modelled in Aspen Plus; therefore the overall reaction was used in the simulation. Reactions [1], [2] and [5] were specified in the 'ANODE' block and it was assumed that they reach equilibrium at the operating temperature (T_{op} = 910 °C). The stream 'AIR' is fed to 'COMP2', the air compressor and its discharge pressure was set to P_{SOFC}. The air composition and thermodynamic condition were inputted and the molar flow rate is set by varying the air flow until the air utilisation factor U_a = 0.167 (7). The compressed air is preheated in 'AIRHEAT' and its exit stream enters 'HEATX1' where it is preheated further by the hot combustion plenum products. Stream 15 enters the 'CATHODE' block, whose function is to separate out the O_2 required for the electrochemical reaction ($nO_{2,consumed}$). The block O_2 split fraction is set using the following equations: $U_f = nH_{2,consumed}/nH_{2,in}$ where $nH_{2,consumed}$ is calculated, $nO_{2,consumed} = 0.5nH_{2,consumed}$ and O_2 split fraction = $nO_{2,consumed}/nO_{2,in}$, which is equivalent to U_a. The fuel utilisation factor (U_f) is known and the $nH_{2,in}$ term is calculated using: $nH_{2,in} = nH_{2,syn\text{-}gas} + 1(nCO_{syn\text{-}gas}) + 4(nCH_{4,syn\text{-}gas}) + \ldots$ where $nH_{2,syn\text{-}gas}$ is the molar flow rate of H_2 contained in 'SYN-GAS'; $1(nCO_{syn\text{-}gas})$ is the molar flow rate of H_2 that could be produced from the CO in 'SYN-GAS'; $4(nCH_{4,syn\text{-}gas})$ is the molar flow rate of H_2 that could be produced from the CH_4 in 'SYN-GAS' and the same applies to the higher hydrocarbons. The required O_2 is directed to the 'ANODE' block. The temperature of the depleted air (stream 17) is brought up to T_{op} in 'HEATER2'. The heat is supplied by the electrochemical reaction, which was simulated by taking a heat stream (Q3) from 'HEATER2' to 'ANODE'. Stream 7 enters the block 'SPLIT', whose function is to split the stream into a recycle and a stream directed to the combustion plenum. The split fraction is determined by a specified *STCR*, defined as the molar ratio of steam to combustible carbon. Excess steam as well as increasing the concentration of H_2 and CO_2 inhibits the formation of carbon.

Carbon deposition not only represents a loss in the system but results in deactivation of catalysts and decreases the activity of the anode by clogging the active sites. The depleted fuel and oxidant are fed to 'POSTCOMB' where complete combustion of the remaining fuel occurs. The heat generated is represented by the heat stream Q5, which is fed to 'HEATER1', whose function is to set the combustion products temperature. Finally, the combustion products (stream 11) serve to preheat the incoming air in the 'HEATX1' block. The temperature of the stack exhaust (stream 12), which may be utilised in a district heating system, is also determined.

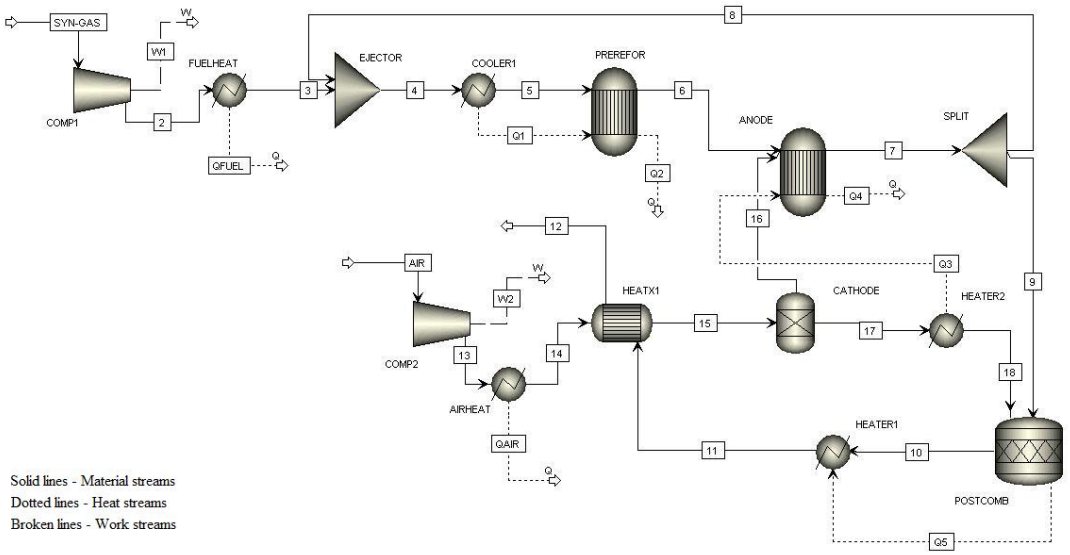

Figure 1. Aspen Plus model flowsheet.

Voltage Calculation

The cell voltage was calculated by first applying the Nernst equation, Equation [6] Table I, and then subtracting the various losses, including ohmic, activation and concentration losses. $\Delta\bar{g}_f$ is the molar Gibbs free energy of formation (J/mol) at standard pressure (1 bar), 2 represents the number of electrons produced per mole of H_2 fuel reacted, F is the Faraday constant (C/mol), T_{avg} is the average temperature between the SOFC inlet and outlet streams (K), R_g is the molar gas constant (J/mol K) and P_i is the partial pressure (bar) of gaseous component i. The partial pressures were taken as average values of the anode and cathode inlet and outlet streams.

The ohmic loss, which is the voltage loss due to the resistance to electron flow through the electrodes and interconnection and the resistance to ion flow through the electrolyte, was calculated using Equations [7] – [10]. These equations developed by Song et al. (17) take into account realistic electron/ion paths. The angle related to the extent of electrical contact is $A\pi$ radians while the angle $B\pi$ radians is related to the interconnection. The resistivity terms (ρ_i) were determined using the temperature dependent relations proposed by Bessette et al. (8). D_m is the mean diameter of the cell (m), t_i is the cell component thickness (m) and w_{Int} is the interconnection width (m). The ohmic loss is especially important for tubular SOFCs as it is the dominant loss due to long current flow paths.

TABLE I. Voltage Calculation Equations.

Reversible Nernst voltage		
Nernst equation	$V_N = -\frac{\Delta \bar{g}_f}{2 \cdot F} + \frac{R_g \cdot T_{avg}}{2 \cdot F} \ln \frac{P_{H_2} \cdot P_{O_2}^{0.5}}{P_{H_2O}}$	[6]
Ohmic loss		
Anode	$V_{Ohm\_A} = \frac{j \cdot \rho_A (A \cdot \pi \cdot D_m)^2}{8 \cdot t_A}$	[7]
Cathode	$V_{Ohm\_C} = \frac{j \cdot \rho_C (\pi \cdot D_m)^2}{8 \cdot t_C} \cdot A[A + 2(1 - A - B)]$	[8]
Electrolyte	$V_{Ohm\_E} = j \cdot \rho_E \cdot t_E$	[9]
Interconnection	$V_{Ohm\_Int} = j \cdot \rho_{Int} (\pi \cdot D_m) \frac{t_{Int}}{w_{Int}}$	[10]
Activation loss		
Anode	$\frac{1}{R_{Act\_A}} = \frac{2 \cdot F}{R_g \cdot T_{op}} \cdot k_A \left(\frac{P_{H_2}}{P^0}\right)^m \exp\left(\frac{-E_A}{R_g \cdot T_{op}}\right)$	[11]
Cathode	$\frac{1}{R_{Act\_C}} = \frac{4 \cdot F}{R_g \cdot T_{op}} \cdot k_C \left(\frac{P_{O_2}}{P^0}\right)^m \exp\left(\frac{-E_C}{R_g \cdot T_{op}}\right)$	[12]
Concentration loss		
Anode	$V_{Conc\_A} = -\frac{R_g \cdot T_{op}}{2 \cdot F} \ln\left[\frac{1 - (R_g \cdot T_{op} / 2 \cdot F)(t_A / D_{An(eff)} \cdot y^0{}_{H_2} \cdot P_{SOFC}) j}{1 + (R_g \cdot T_{op} / 2 \cdot F)(t_A / D_{An(eff)} \cdot y^0{}_{H_2O} \cdot P_{SOFC}) j}\right]$	[13]
Cathode	$V_{Conc\_C} = -\frac{R_g \cdot T_{op}}{4 \cdot F} \ln\left[\frac{(P_{SOFC} / \delta_{O_2}) - ((P_{SOFC} / \delta_{O_2}) - y^0{}_{O_2} P_{SOFC}) \exp[(R_g \cdot T_{op} / 4 \cdot F)(\delta_{O_2} \cdot t_C / D_{Cat(eff)} \cdot P_{SOFC}) j]}{y^0{}_{O_2} \cdot P_{SOFC}}\right]$	[14]
Actual voltage	$V = V_N - (V_{Ohm} + V_{Act} + V_{Conc})$	[15]

The activation loss due to slow or sluggish kinetics of the electrochemical reaction was determined using semi-empirical correlations, Equations [11] and [12] (18). The R_{Act_i} terms represent specific resistance (Ω m^2) at both anode and cathode. The activation voltage loss V_{Act_i} was evaluated by multiplying the specific resistance terms by j (A/m^2). The pre-exponential factors k_i and activation energies E_i are given in Achenbach (18). The partial pressures P_i (bar) were taken as average values of the anode and cathode inlet and outlet streams. P^0 is a reference pressure and was taken as 1 bar; the influence of partial pressure is accounted for by the slope m. The activation voltage loss is less significant in SOFCs compared to other fuel cells due to the high operating temperature.

The concentration loss due to mass transfer limitations in the porous electrodes was modelled using Equations [13] and [14] (19). Equations [13] and [14] were derived using Fick's law of diffusion with both ordinary and Knudsen diffusion considered. Both types of diffusion were accounted for by calculating effective diffusion coefficients for the anode and cathode ($D_{An(eff)}$ and $D_{Cat(eff)}$). The explanation of methods for calculating diffusion coefficients is beyond the scope of this paper. The Fuller et al. method (20) was applied to determine the ordinary binary diffusion coefficients and the method reported by Chan et al. (19) was used to calculate the Knudsen diffusion coefficients and overall effective diffusion coefficients. The anode and cathode effective diffusion coefficients and δ_{O2} were calculated using equations reported in Chan et al. (19). The $y^0{}_i$ terms in Equations [13] and [14] are the gas molar fractions in the bulk flow, taken as the average values of the anode and cathode inlet and outlet streams. This loss is low unless the current density is high and the fuel and air concentrations are low, caused by high utilisations. Under these conditions the limiting current may be reached reducing the fuel cell voltage to very low levels.

Finally, the actual voltage V was calculated using Equation [15], which is simply the Nernst voltage less the sum of the voltage losses. The voltage calculations are carried out using a design spec, which varies the input fuel flow rate until the DC power ($P_{el,DC} = VI$) equals a specified value (base case: 120 kW). However, for known current (I), as was the case for the current density sensitivity analysis, a calculator block sets the input fuel flow using: $n\mathrm{H}_{2,\mathrm{in}}$ (kmol/h) = $(I/2FU_f)(3600/1000)$ and $n\mathrm{Fuel}_{\mathrm{in}}$ (kmol/h) = $n\mathrm{H}_{2,\mathrm{in}}/(y\mathrm{H}_2 + y\mathrm{CO} + 4y\mathrm{CH}_4 + \ldots)$ where y_i is the molar fraction of gaseous component i, then V and $P_{el,DC}$ are calculated. In both cases, the gross and net AC efficiencies (LHV basis) are determined. The gross AC efficiency is defined as: $\eta_{el,gross} = P_{el,AC}/(n\mathrm{Fuel}_{\mathrm{in}}\mathrm{LHV}_{\mathrm{fuel}})$ where $P_{el,AC}$ is the AC power (kW), $n\mathrm{Fuel}_{\mathrm{in}}$ is the molar flow rate of input fuel (kmol/s) and $\mathrm{LHV}_{\mathrm{fuel}}$ is the lower heating value of the input fuel (kJ/kmol). The net AC efficiency is defined as: $\eta_{el,net} = (P_{el,AC} - P_{comp})/(n\mathrm{Fuel}_{\mathrm{in}}\mathrm{LHV}_{\mathrm{fuel}})$ where P_{comp} is the electrical power requirement of the fuel and air compressors (kW).

Model Validation

Validation of the model against published data for the SPGI 100 kW CHP SOFC stack operating on natural gas was carried out.

TABLE II. Model Validation.

	Published data (21)	**Model results**
Voltage (V)	0.7	0.683
Current density (A/m^2)	1780	1828.6
Pre-reforming temperature (°C)	536	535.1
Pre-reformer CH_4 conversion fraction	0.259	0.25
Anode exhaust gas composition (mole %)	H_2 11.6, CO 7.4, H_2O 50.9, CO_2 24.9, N_2 5.1	H_2 11.6, CO 7.4, H_2O 50.9, CO_2 24.9, N_2 5.1
Cathode inlet temperature (°C)	821.32	823.7
Cathode exhaust gas composition (mole %)	O_2 17.7, N_2 82.3	O_2 17.7, N_2 82.3
Combustion products temperature (°C)	1012.35	1012.3
Stack exhaust temperature (°C)	833.85	833.7
Stack exhaust gas composition (mole %)	H_2O 4.5, CO_2 2.3, O_2 15.9, N_2 77.3	H_2O 4.5, CO_2 2.3, O_2 15.9, N_2 77.3
Gross AC efficiency (LHV) (%)	52	51.28
Net AC efficiency (LHV) (%)	-	49.15

During validation runs the model inputs were as follows (9, 21):

- Natural gas composition (mole %): CH_4 81.3%, C_2H_6 2.9%, C_3H_8 0.4%, C_4H_{10} 0.2%, N_2 14.3%, CO_2 0.9%.
- Operating pressure (P_{SOFC}) / ejector pressure ratio: 1.08 atm. / 3.
- Operating / anode and cathode exhaust temperature (T_{op}): 910 °C.
- Input air / fuel temperature: 630 / 200 °C.
- U_f / U_a / $STCR$: 0.85 / 0.19 / 1.8.
- DC power ($P_{el,DC}$) / DC to AC inverter efficiency: 120 kW / 92%.

The model results are in good agreement with published data (see Table II). There is only a slight difference for voltage, current density and efficiency. The reader should note that Zhang et al. (21) used a very different method for calculating the voltage to the one applied in this work. They used semi-empirical correlations developed using a reference polarisation curve. For comparison, Campanari (9) reports a voltage and current density of 0.69 V and 1800 A/m^2 and a net AC efficiency of 48.5%. These results compare well with this work.

Results and Discussion

The model was run using the syn-gas compositions for wood and miscanthus fuel given in the 'Biomass Gasification Systems' section of this paper. The input data was kept the same as for validation with the following exceptions: fuel temperature = 300 °C, U_a = 0.167 and *STCR* = 2.5. As expected stack performance was better on natural gas than syn-gas. For the wood case gross and net efficiency reduced 8.28% and 11.63% to 43% and 37.52% respectively at j = 1828.6 A/m^2. For miscanthus gross and net efficiency reduced 9.63% and 15.9% to 41.65% and 33.25% respectively. The drop in efficiency for syn-gas fuel is attributed to increased required fuel and air input, which is due to the lower quality of the fuel gas and also decreased power. Even with this performance decrease the efficiency achieved is much higher than traditional biomass systems.

Figure 2 displays the voltage characteristics of a single tubular SOFC fed with (a) wood syn-gas and (b) miscanthus syn-gas. The predicted voltage characteristics are consistent with well known phenomena for tubular SOFCs: Nernst voltage = ~0.9 V; ohmic loss is dominant; activation loss is less significant in SOFCs due to high temperature; concentration loss is the least significant but increases rapidly at high current density. Voltage characteristics were found to be better for wood than miscanthus, due to greater voltage losses in the miscanthus case. For example, at a typical j of 1900 A/m^2 the cell voltage for wood syn-gas is 0.66 V and for miscanthus syn-gas it is lower at 0.637 V.

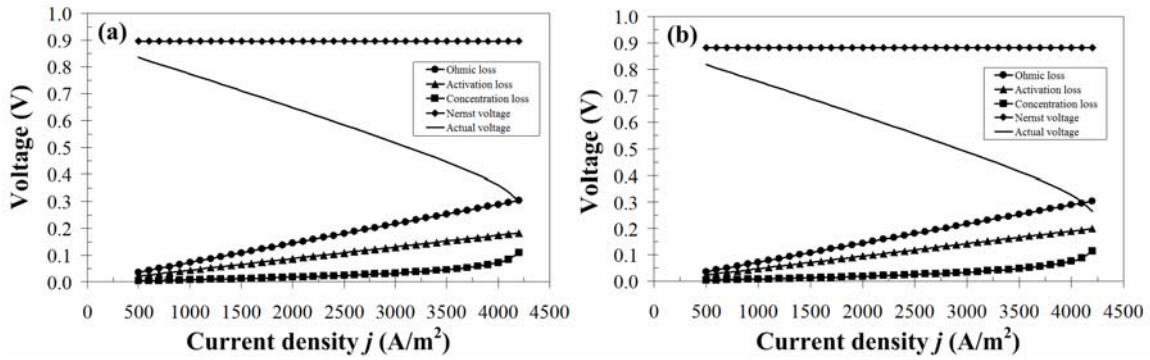

Figure 2. SOFC voltage characteristics versus current density for (a) wood syn-gas and (b) miscanthus syn-gas.

Effect of Current Density

From Figure 3 it is evident that j has significant influence on the system for both fuels. Increasing j lowers both voltage and efficiency but increases power. Voltage is reduced as a result of increased losses as shown in Figure 2. Efficiency drops substantially (~35%

for both fuels) due to higher parasitic power and energy input. Power increases to a maximum and then decreases. Fuel cells are usually operated to the left of this point. It is desirable with regard to operating costs, to operate the stack at high voltage and efficiency; however it is also desirable with regard to capital costs, to operate the stack at high power. Therefore there must be a trade-off between voltage, efficiency and power. The stack operates with better performance on wood syn-gas compared to miscanthus syn-gas. The miscanthus syn-gas fed to the stack had much lower H_2 and higher CO_2, H_2O and N_2 content than the wood syn-gas, which caused the reduction in performance. It also meant that a much higher fuel flow rate was required for the miscanthus case.

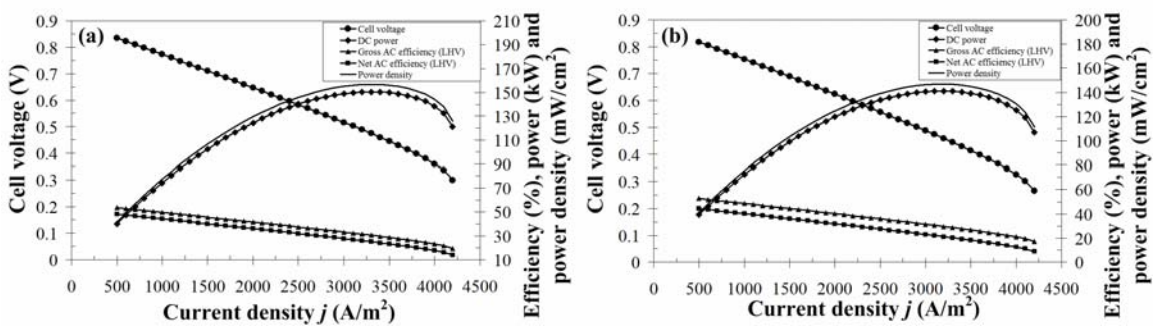

Figure 3. Effect of current density on voltage, power and efficiency for (a) wood syn-gas and (b) miscanthus syn-gas.

Effect of Steam to Carbon Ratio

The effects of changes in *STCR* are displayed in Figure 4. *STCR* has a substantial impact on the pre-reformer, the inlet temperature increases approximately 320 °C over the *STCR* range for both cases due to the recirculation of more high temperature depleted fuel. As a result the anode temperature rises and causes greater CH_4 conversion (0 to 92.2% and 0 to 97% for wood and miscanthus respectively). The high temperature and greater amount of steam available promotes the steam reforming of CH_4 via reaction [1]. This reaction is endothermic meaning the forward reaction is favoured as temperature increases. Increasing *STCR* had a negative impact on voltage and efficiency, which was due to the change in anode temperature and gaseous component partial pressures causing the Nernst voltage to decrease and the voltage losses to rise. It is therefore desirable to operate the stack at low *STCR*; however it should be high enough to inhibit carbon formation.

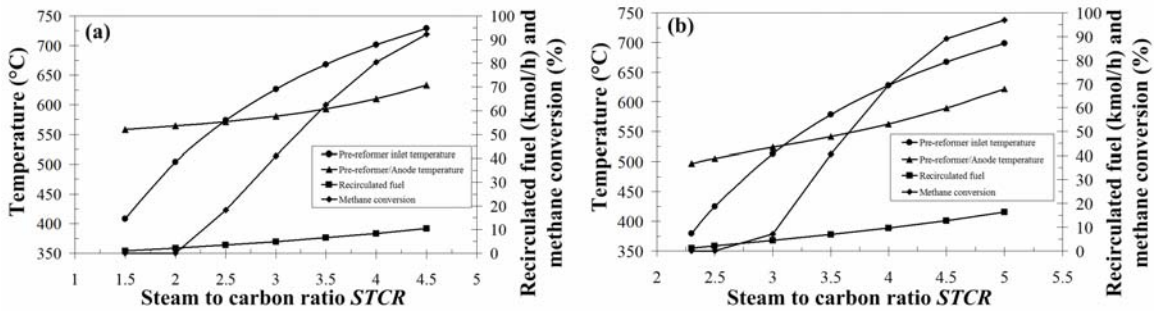

Figure 4. Effect of steam to carbon ratio for (a) wood syn-gas and (b) miscanthus syn-gas.

Effect of Fuel Utilisation Factor

Figure 5 depicts the influence of U_f on stack performance for miscanthus syn-gas fuel. The cell voltage decreases with U_f due to increased voltage losses. The input fuel required to achieve the desired power decreases with U_f because more of the fuel energy is converted to electricity rather than heat. Efficiency increases significantly (~17%) as a result of the reduced fuel input. The amount of recirculated fuel decreases with U_f as less fuel needs to be recirculated to meet the specified *STCR* due to the increased H_2O content in the depleted fuel. As a result of less high temperature depleted fuel being recirculated the pre-reformer/anode temperature drops. The cathode and stack exhaust temperatures are dependent on the combustion temperature, which is determined by the amount of fuel available to the combustion plenum. At low U_f more of the fuel is available for combustion therefore the temperatures are high and as U_f increases the temperatures decrease. The SOFC stack should be operated at high U_f but below the level where the concentration loss increases to a high degree.

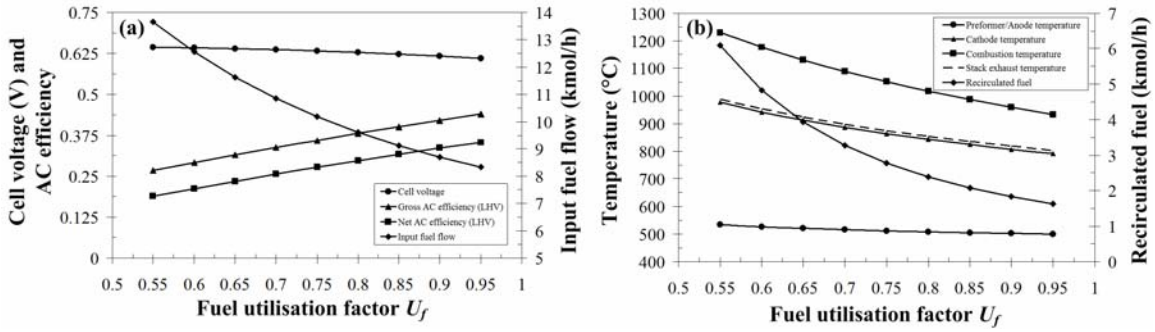

Figure 5. Effect of fuel utilisation factor for miscanthus fuel on (a) voltage, efficiency and input fuel flow and (b) pre-reformer/anode temperature, cathode temperature, combustion temperature, stack exhaust temperature and recirculated fuel.

Effect of Air Utilisation Factor

The influence of U_a on the system for wood syn-gas is shown in Figure 6. The cell voltage and gross efficiency decrease with U_a and the current density increases. The influence of U_a is much less significant than that of U_f. The net efficiency rises and reaches a peak value at a U_a of ~20% and then decreases. For this reason SOFCs should be operated in the U_a range: 16 to 20%. As displayed in Figure 6 (b) the stack temperatures rise with U_a, the reason being that at high U_a less air is fed to the stack which means there is less N_2 and excess O_2 for cooling in the combustion plenum.

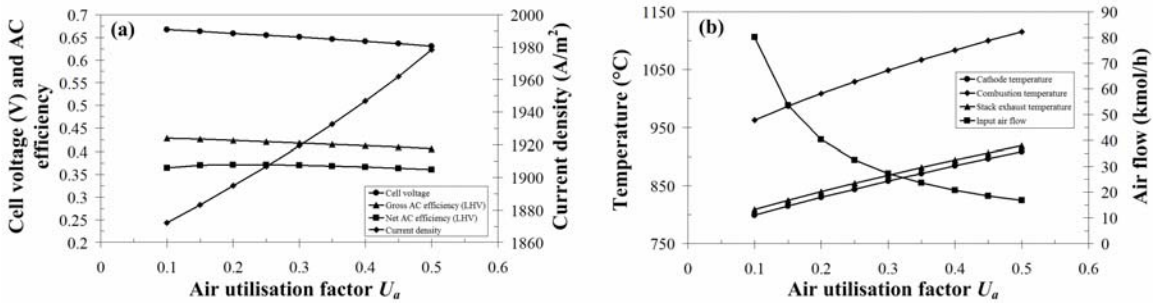

Figure 6. Effect of air utilisation factor for wood fuel on (a) voltage, efficiency and current density and (b) cathode temperature, combustion temperature, stack exhaust temperature and input air flow.

Conclusions

A model of the SPGI 100 kW CHP tubular SOFC stack was developed using Aspen Plus. The objective of the work, which was to develop a computer simulation model of a BG-SOFC CHP system capable of predicting system performance under various operating conditions and using diverse fuels, was achieved. The model uses existing Aspen Plus unit operation blocks with minimum requirements for linking of a subroutine thus reducing complexity and ensuring short computational times. It was validated against published data. The effects of varying j, $STCR$, U_f and U_a on SOFC stack performance were investigated for the stack operating on wood and miscanthus syn-gas. The results indicate that there must be a trade-off between voltage, efficiency and power with respect to j and the stack should be operated at low $STCR$ and high U_f. Also, the stack should be operated at a U_a of ~20%. Operation on biomass syn-gas was compared to natural gas operation and as expected performance degrades. Better stack performance was observed for wood syn-gas compared to miscanthus syn-gas, the main reason being the higher H_2 content of the wood syn-gas. The reduction in efficiency seen for syn-gas operation is attributed to increased required fuel and air input, which is due to the lower quality of the fuel gas and also decreased power. Even with this performance decrease the efficiency achieved is much higher than traditional biomass systems, making this technology very promising.

References

1. T. Seitarides et al., *Renewable Sustainable Energy Rev.*, **12**, 1251 (2008).
2. S. Cordiner et al., *Appl. Therm. Eng.*, **27**, 738 (2007).
3. L. Fryda et al., *Energy Convers. Manage.*, **49**, 281 (2008).
4. K. D. Panopoulos et al., *J. Power Sources*, **159**, 570 (2006).
5. T. Pröll et al., ASME Turbo Expo: Power for Land, Sea, and Air/2004.
6. M. Sucipta et al., *J. Fuel Cell Sci. Technol.*, **5**, 041006-1-8 (2008).
7. R. Suwanwarangkul et al., *J. Power Sources*, **166**, 386 (2007).
8. N. F. Bessette et al., *J. Electrochem. Soc.*, **142**, 3792 (1995).
9. S. Campanari, *J. Power Sources*, **92**, 26 (2001).
10. A. Bharadwaj et al., *J. Fuel Cell Sci. Technol.*, **2**, 38 (2005).
11. M. Cali et al., *Int. J. of Hydrogen Energy*, **32**, 343 (2007).
12. S. Kakaç et al., *Int. J. of Hydrogen Energy*, **32**, 761 (2007).
13. G. Schuster et al., *Bioresour. Technol.*, **77**, 71 (2001).
14. T. Pröll, Private Communication, Vienna University of Technology, 2008.
15. M. Siedlecki et al., World Renewable Energy Congress IX/2006.
16. M. Siedlecki, Private Communication, Delft University of Technology, 2009.
17. T. W. Song et al., *J. Power Sources*, **142**, 30 (2005).
18. E. Achenbach, *J. Power Sources*, **49**, 333 (1994).
19. S. H. Chan et al., *J. Power Sources*, **93**, 130 (2001).
20. E. N. Fuller et al., *Ind. Eng. Chem.*, **58**, 19 (1966).
21. W. Zhang et al., *Energy Convers. Manage.*, **46**, 181 (2005).